Two-Step Photoexcitation Mechanism in Amorphous Se

J. Berashevich, A. Mishchenko, and A. Reznik

Thunder Bay Regional Research Institute, 290 Munro Street, Thunder Bay, Ontario P7A 7T1, Canada
Department of Physics, Lakehead University, 955 Oliver Road, Thunder Bay, Ontario P7B 5E1, Canada

(Received 29 January 2014; revised manuscript received 31 March 2014; published 28 April 2014)

The first-principles simulations are applied to study a photoinduced metastability in amorphous selenium and contribution of the valence-alteration pair (VAP) defects in this process. The VAP defect is confirmed to be the equilibrium defect; it minimizes the destabilizing interaction induced by disorientation of the lone-pair (LP) electrons along the Se chains, and, thus, relieves tension in a system. The photoexcitation involves the LP electrons, and it is proposed to be described by two coexisting processes, namely, single- and double-electron excitations. Both processes are found to induce the defect states in the band gap and cause experimentally observed photodarkening; however, only double-electron excitation is capable of triggering bond rearrangement and structural transformation. Lattice relaxation, which follows bond rearrangement, occurs with characteristic energy of -0.9 ± 0.3 eV. It is found to promote formation of energetically favorable VAP defects and to trigger the ringlike to helixlike transformations, thus, ultimately stimulating the photoinduced crystallization. The photoinduced crystallization is directly simulated in a system characterized by increased crystalline order.

DOI: 10.1103/PhysRevApplied.1.034008

I. INTRODUCTION

The progressively expanding area of applications of chalcogenide glasses (from medical imaging detectors to phase-change memories) supports a continuous interest in their properties, one of which is photoinduced transformation—a very unique phenomenon inherent to chalcogenide glasses including amorphous Se (*a*-Se). The transformation is known to be triggered by optical or x-ray irradiation and is associated with a creation of defects [1–3]. The most studied defect in amorphous Se is a valence-alteration pair (VAP) [1–5] which belongs to "equilibrium-type" defects [4], meaning that VAP exists in well-relaxed structure prior to photoexcitation. However, photoexcitation is assumed to enhance a concentration of the VAP defects by initiating the bond breaking reaction: $2C_2^0 \leftrightarrow C_3^+ + C_1^-$, where C_2^0 is a selenium atom in its normal twofold configuration, C_3^+ is a positively charged threefold configuration, and C_1^- is a negatively charged onefold coordinated Se atom [1]. The experimentally detected unpaired electrons, which appear upon illumination, are considered to be direct evidence of the valence alteration in *a*-Se [2]. It is believed that the VAP defects are responsible for many of the photoinduced effects including photodarkening (PD) [6–8], photoinduced crystallization [7], and volume expansion [9–11], as they induce the sub-band-gap defect states [12–15]. Although a link between these effects is not confirmed with direct experiments, they all have comparable kinetics and are shown to be thermally activated processes with similar activation energies around 0.8–0.9 eV [6,7]—the value which is suggested for relaxation of the VAP defect [16].

In order to get better insight into the nature of the photoinduced effects and contribution of the VAP defects in it, we model the entire process of photoexcitation with the help of the first-principles methods. First, we classify all possible VAP defects in an *a*-Se network, their energetics, and positions in the band gap. Then, we simulate a photoexcitation from an ideal system (consisting of strictly twofold coordinated Se atoms) and a system containing the VAP defect. We show that in both systems, the excitation of two electrons from the lone-pair (LP) state may trigger a formation of a dynamic bond with the characteristic energy of -0.9 ± 0.3 eV through the photoinduced relaxation of the immediate neighborhood. In the postexcitation regime, this dynamic bond is broken, which then induces the bond rearrangement followed by a creation either of the VAP defect or the crystalline inclusion. In contrast, the removal of just one electron from the LP state does not generate any significant lattice relaxation and, therefore, does not lead to a permanent structural transformation. The simulated photoinduced transformations show good correlation with the PD kinetics measured under the red light illumination. The comparison with the experimental results suggests that the slow component in the kinetics of the photodarkening relaxation can be linked to the process which involves bond rearrangements (i.e., when two electrons are photoexcited from the LP state) with the experimentally found activation energy $E_B = 0.8 \pm 0.1$ eV. In contrast, the fast component in the photodarkening relaxation characterizes a process which does not involve any significant lattice relaxation, and, in accordance with simulations, is originated from a single-electron excitation.

II. THEORETICAL METHODS

For our study, we create the model compounds of amorphous Se consisting of 25 and 50 atoms. For the atomistic simulations, the WIEN2K package [17] with implementation of the Perdew-Burke-Ernzerhof parametrization of the generalized gradient approximation [18] is used. The optimization procedure is carried out using a minimization of forces for which the product of atomic sphere radius (1.8 bohr centered at the nucleus of the individual atoms) and the plane-wave cutoff in k space is set to 7. The Brillouin zone of a supercell of 25 atoms is covered by the $4 \times 4 \times 4$ Monkhorst-Pack mesh. The size of the Monkhorst-Pack mesh is adjusted to the supercell size; i.e., the mesh is appropriately reduced as the supercell is enlarged. The energy separating the core and valence electrons is set to -6.0 Ry. The force tolerance 0.5 mRy/bohr in combination with tight convergence limits (energy convergence 0.0001 Ry, force convergence 0.1 mRy/bohr, and charge convergence $0.001e$) are applied.

To study the fundamental properties of a-Se including the formation of the VAP defects and photoinduced structural transformations, the well-amorphized structure of a-Se placed in a cubic supercell ($\alpha = 90°$, $\beta = 90°$, $\gamma = 90°$) is used (the size of the cubic supercell consisting of 25 atoms is $8.7\ \text{Å} \times 8.7\ \text{Å} \times 9.9\ \text{Å}$). The periodic boundary conditions are applied to the supercell. For the simulation of the photoinduced crystallization, the system of the increased crystalline order is created, and it is assigned to recognize the symmetry of trigonal Se (t-Se) through application of the hexagonal lattice parameters to the supercell ($\alpha = 90°$, $\beta = 90°$, $\gamma = 120°$).

In order to ensure that the adjacent replicas of the supercell do not interact, the results achieved for a supercell of 25 atoms is reexamined with a bigger supercell of 50 atoms. The main focus is on the effect of the supercell size on the interaction between the VAP defects (it is known that charged centers are responsible for intercell interactions). It is found that due to the strong localization of the defect states, their intercell interactions are negligibly small. Indeed, the localization length of a photogenerated hole at the VAP defect does not exceed 10 Å, as a hole is delocalized over four to five sites only. In such, a localized state at the VAP defect is confined within the boundaries of a supercell of 25 atoms, and supercell enlargement does not affect our simulations.

III. DEFECT-FREE SYSTEM

We start our analysis from an ideal amorphous Se system containing only twofold coordinated Se atoms, each having two electrons on the p-bonding orbital, two empty quantum states on the p-antibonding orbital, and two electrons on the nonbonding LP orbital. The properties of such ideal network are governed by the lone pairs: by pushing the shared orbitals apart, they define the bond angle and torsion angle. The crystalline systems, i.e., trigonal and α-monoclinic Se, are built in a way to minimize interatomic interactions of the LP electrons. In an amorphous network, LPs are disoriented, which causes repulsion between them resulting in tension along the chain. Therefore, the total energy of a-Se is increased by $\Delta = 0.08$ eV per atom in comparison with t-Se. The charge exchange between Se atoms in an amorphous network (up to $\pm 0.5\ \bar{e}$ per atom) is an attempt to reduce tension along the chains.

An example of an ideal structure with two adjacent polymerlike chains is shown in Fig. 1. The bond length between the twofold coordinated sites varies in the range of 2.30–2.47 Å, which agrees well with an average bond length in a-Se of 2.37 Å found previously [9,16]. The interatomic distance between the atoms that are not involved in a covalent bond formation varies in a wide range with a lower limit at 2.80 Å (see Fig. 1). The twofold coordinated model is consistent with many other theoretical simulations [9,19,20] and agrees with the experimental data [21,22]. It should be noted that if the average bond length is enlarged to 2.80 Å, some atoms can be considered as threefold coordinated (see Fig. 1). Indeed, overcoordinated defects are suggested to be common in Se structure [23,24].

As it can be seen from Fig. 1, polymerlike Se chains are built from helixlike and ringlike segments which are needed to reduce repulsion between LP orbitals. In our model compound, the helixlike character dominates over the ringlike one. It correlates well with the previous study [19] showing that the helixlike configuration is energetically favorable: the energy gain upon the ringlike to helixlike transformation can be up to -0.025 eV per atom. As it was shown in Ref. [19], for a ringlike segment consisting of seven atoms, large repulsion occurs when its tails tend to overlap. Therefore, it is expected that the formation of a closed ring instead of overlapping tails should reduce repulsion and suppress tension along the chain. To confirm this, we compare the total energies of a network containing a closed-ring configuration with an

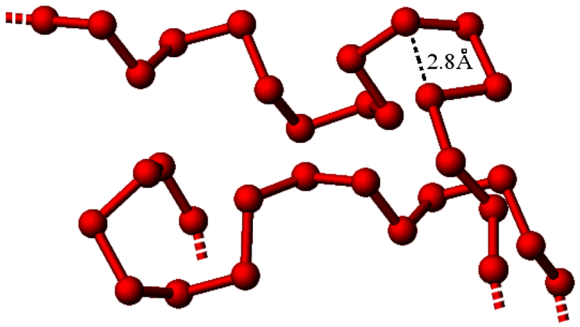

FIG. 1. The structural model of an ideal system of a-Se presented by two adjacent chains: the shortest interatomic distance of 2.80 Å between atoms, which are not involved in covalent bond formation, is indicated. The periodic boundary conditions allow the infinite chains.

ideal network. The size of the closed-ring configuration is defined by the equilibrium reactions $Se_\infty \leftrightarrow Se_8 \leftrightarrow Se_7 \leftrightarrow Se_6$ [19,20,24,25] (the presence of rings in *a*-Se samples is verified by Raman measurements [26,27]). Following this approach, we simulate the formation of a Se_7 ring, and, indeed, the total energy of a system is decreased by $\Delta = -0.02$ eV per atom (it corresponds to the decrease in the total energy by −0.49 eV).

With respect to the electronic properties, the disorientation of the LPs causes formation of the band tails. The edge of the valence band (E_V) generated by the lone pairs is found to be smeared by the broad tails as defined by $\Delta E_V = E_V + 0.45$ eV. Because the bottom of the conduction band (E_C) is formed by *p*-antibonding orbitals, the effect of LP disorientation is less pronounced there [28], giving a rise to the band tails of size $\Delta E_C = E_C - 0.16$ eV. This simulated asymmetry in the band tails has also been observed experimentally [12,13].

To demonstrate an effect of chain tension on the band tails' size, a comparison between an ideal system and the one containing the Se_7 ring is made. We find that due to an improvement in the LPs' orientation, the formation of the Se_7 ring reduces the band tails by approximately 0.3 eV in total, with the most pronounced effect near the valence band.

IV. THE VAP DEFECTS AND THEIR CLASSIFICATION

In addition to crystallinelike inclusions, another way to resolve destabilizing interactions of the LP orbitals along the chains is chain discontinuation. When the chain breaks, one C_1^0 end remains as the separated site, while another connects to a twofold C_2^0 site of another chain, thus, becoming a threefold C_3^0 [see the defect structure in Fig. 2(a)]. This process is followed by the charge exchange reaction $C_3^0 + C_1^0 \rightarrow C_3^+ + C_1^-$ [see the charge distribution in Fig. 2(a)] and formation of a two-chain VAP defect [2,3]. We find that the total energy lowering with this defect formation is $\Delta = -0.05$ eV per atom (it corresponds to a decrease in the total energy by −1.22 eV as compared to an ideal structure). Therefore, we numerically confirm that the two-chain VAP defect is very efficient in relieving the tension along the chains despite a strong dipole formed between the C_3^+ and C_1^- sites. With respect to the defect structure, the C_3^+ and C_1^- sites are separated by a distance 3.15 Å, while the bond length around C_3^+ is slightly elongated to 2.4–2.6 Å due to the bond iconicity.

When the broken C_1^0 end connects to the same chain, another type of VAP defect emerges [see Fig. 2(b)] [5], which is named in the literature as the "intimate" VAP defect (IVAP) [5]. The IVAP defect appears on a single chain of an ideal network and does not affect the electronic and structural configurations of the other chains. We find that the IVAP defect is stable only in the intimate configuration. The mechanism of formation of the IVAP defect is the same as for the VAP [Fig. 2(a)]: one broken end remains detached while a second attempts to convert into a threefold site denoted in Fig. 2(b) as the C_3^+ site. Because the induced charge redistribution is restricted to a single chain, the originated strong dipole keeps apart the C_3^+ and C_{13}^- sites at a distance $d_{C_{13}^- - C_3^+} = 2.82$ Å, i.e., the third bond associated with the C_3^+ site is elongated [see the dashed line in Fig. 2(b)]. Moreover, a strong dipole moment masks the stress-relieving effect, and as a result, no decrease in energy is detected with the formation of this defect. However, when two IVAP defects appear in a pair [see Fig. 2(c) showing two IVAP defects separated by a distance of approximately 3.8 Å], the interaction between the defects reduces the total dipole moment. The bond between the C_{13}^- and C_3^+ sites shortens to $d_{C_{13}^- - C_3^+} = 2.78$ Å, and the total energy decreases by $\Delta = -0.04$ eV per atom uncovering the stress-relieving effect. Therefore, the IVAP pair is more stable than the single IVAP defect (the total energy difference is −1.08 eV), and the IVAP defects are expected to appear predominantly in pairs. It should be noted that the structural rearrangements with IVAP pair formation are confined within two involved chains only [see Fig. 2(c)] and do not affect the rest of the network.

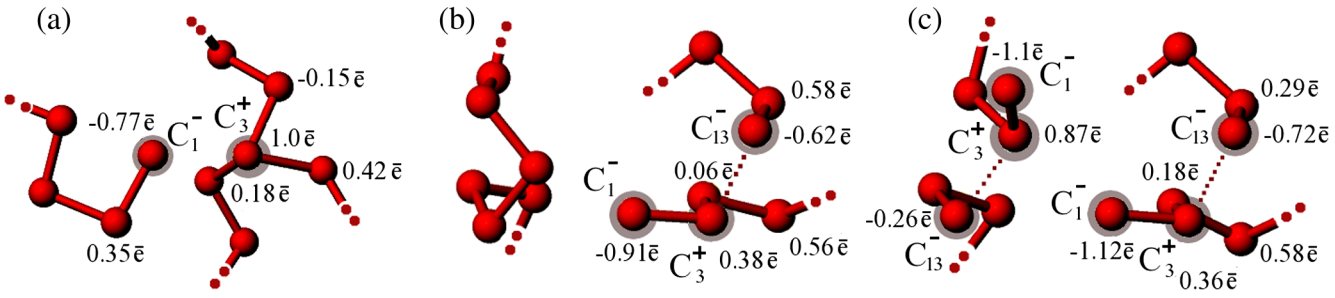

FIG. 2. The VAP defects with a distribution of a net charge (a) two-chain VAP defect. (b) Single IVAP defect; the C_3^+ site corresponds to the threefold coordinated site for which the third bond between the C_{13}^- and C_3^+ sites is elongated (denoted by the dashed line) due to the strong dipole moment. (c) Pair of IVAP defects; the bond between the C_{13}^- and C_3^+ sites is shortened as the defect dipoles are partially compensated due to defect pairing.

Overall, we find an ideal defect-free system to be the highest in energy. The VAP defects or crystalline inclusions like closed rings [20,27,29] are thermodynamically favorable [4], since they reduce the stress originated from the LPs disorientation, and there will be always an interplay between the rings and the VAP defects. Preference is given to the formation of the VAP defects [Fig. 2(a)], as they are more effective in relieving tension along the chains, which is reflected in the largest energy reduction of $\Delta = -0.05$ eV per atom. Not willing to speculate about the concentration of the VAP defects (to the best of our knowledge, there is no viable theoretical approach to estimate the concentration of the equilibrium sites), we expect that the higher concentration of sites relieving tension along the chains will be present in amorphous Se layers with enhanced strain, for example, at an interface with a solid substrate.

The VAP defects have a direct impact on the electronic properties of a-Se. According to our calculations, the defect states generated by C_3^+ appear below the conduction band at $E_C - 0.33$ eV for the two-chain VAP, at $E_C - 0.43$ eV for the single IVAP, and at $E_C - 0.61$ eV for the IVAP pair. The energetic positions of the defect states induced by C_3^+ agree well with the experimental observation showing two peaks in the density of states at approximately 0.30 eV and 0.45–0.50 eV below E_C [13], which is also consistent with the positions of the charged centers in Ref. [14]. The C_1^- states are located above the valence band at $E_V + 0.34$ eV for the VAP and the single IVAP defects and at $E_V + 0.23$ eV for the IVAP pair. Therefore, the C_1^- states appear inside the valence band tails defined by $\Delta E_V = E_V + 0.45$ eV. Depending on the concentration of the VAP, single IVAP, and IVAP pairs, they may influence the density-of-state distribution causing characteristic features at about 0.23 and 0.34 eV above the valence band, as observed in some experiments [12].

Therefore, our finding confirms that the VAP defects are the thermodynamic or the "equilibrium" type as suggested in the literature [4]; i.e., they should be present in high concentration in well-relaxed structures even prior to light exposure. According to the experimental data [2,3], the concentration of the VAP defects is expected to grow under light illumination. Hence, our next step is a simulation of the photoinduced changes in an amorphous Se network with a focus on the formation of the VAP defects.

V. PHOTOINDUCED LATTICE RELAXATION

The photoexcitation process can be described with a potential diagram presented in Fig. 3. The excitation of electrons brings the system from a ground state A to an excited state A^*. We assume that an electron excited into the conduction band leaves behind a hole in the valence band tails. The state in the valence band tails missing one or two electrons induces lattice relaxation of the immediate neighborhood needed for its stabilization. As a result, the excited A^* state converts either into a B^* or C^* state. The B^* state accounts for the insignificant lattice relaxation involving the bond shortening or elongation and in such characterized by a small decrease in energy ΔU_{EB}. In contrast, the C^* state occurs with the bond rearrangements reflected in large ΔU_{EC}. The $A^* \rightarrow C^*$ transition requires overcoming the potential barrier ΔV_B. When the missing electrons return, only the B^* state is able to relax into the original ground state A.

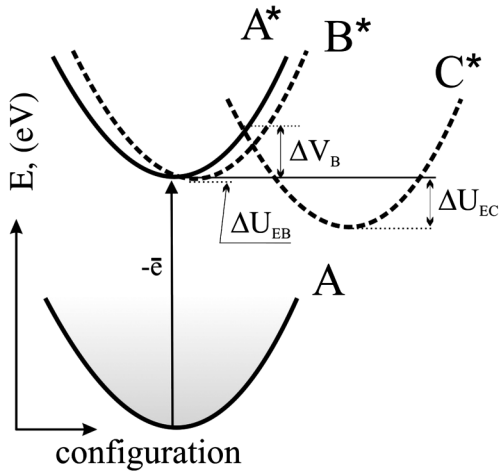

FIG. 3. Potential diagram describing an excitation of the A state and contribution of the photoinduced lattice relaxation into the stabilization of the excited state A^*. The energy scale reflects the total energy of a system.

The sub-band-gap excitation occurs primarily from the top of the valence band formed by the LP electrons: for an ideal system, an excitation involves the partially charged C_2^- sites, while for the VAP defects, the C_1^- sites are those who participate. Upon excitation, the LP occupancy is reduced by one electron ($\mathrm{LP}^2 - \bar{e} \rightarrow \mathrm{LP}^1$), and the LP^1 state with an unpaired electron is shifted deeper into the band gap by approximately 0.2 eV due to an alteration in the exchange interaction upon removal of an electron. The LP^1 states are detected experimentally due to a presence of the unpaired electrons [2] and are known to induce the PD effect. The LP^1 state is delocalized over several sites: our calculations show that it involves up to five sites for the two-chain VAP defect. The relaxation of the immediate neighborhood around the LP^1 state, which is required for its stabilization, is accompanied by the bond shortening or elongation occurring with characteristic energy $\Delta U_{EB} \geq -0.1$ eV that corresponds to the B^* state in Fig. 3. The bond shortening is observed for the IVAP defects [see Figs. 2(b) and 2(c)]. The $d_{C_{13}^- - C_3^+}$ bond shortens by 0.1 Å, which agrees with the previous findings [9]. In contrast, the double-chain VAP defect shows a significant increase in distance between the C_3^+ and C_1^- sites by 0.25 Å. Because the double-chain VAP defects should dominate over other defects, an increase in a separation between the C_3^+ and C_1^-

sites will govern the volume expansion observed experimentally [10]. Since the bond elongation occurs with the characteristic energy ΔU_{EB}, it is not an immediate process. Therefore, the volume expansion caused by the LP^1 states at the double-chain VAP defect is expected to be delayed from the PD onset, which agrees with the experimental observations [10]. When the missing electron returns ($LP^1 + \bar{e} \rightarrow LP^2$), we find that all systems come back to the original state A.

The single-electron excitation described above does not produce any bond rearrangements (causing only either bond elongation or shortening). In order to induce formation of the robust dynamic bond known as the C_3-C_3 defect [2,3], an excitation of two electrons in the vicinity of a single site is required. This is simulated here as a $LP^2 - 2\bar{e} \rightarrow LP^0$ process (LP^0 appears above the LP^1 position in the band gap). Because the excitation of two electrons is unlikely to occur simultaneously, two possible scenarios are considered. (i) $LP^1 - \bar{e} \rightarrow LP^0$: inequality in the charge distribution generated by LP^1 promotes the excitation of the second electron from the vicinity of the same site. (ii) $LP^1 + LP^1 \rightarrow LP^0 + LP^2$: two interacting LP^1 states undergo charge exchange. The latter process is feasible when the energy lowering due to the stabilization of the LP^0 state is greater than $2\Delta U_{EB}$ needed to stabilize two interacting LP^1 states.

The double-electron excitation is simulated by the successive removal of two electrons from the system. For an ideal twofold coordinated system and the IVAP pair defect [Fig. 2(c)], the significant lattice relaxation with the characteristic energy $\Delta U_{EC} = -0.9 \pm 0.3$ eV is followed by the bond rearrangements (the C^* state in Fig. 2). In an ideal twofold coordinated system, the C_3-C_3 dynamic bond occurs through cross-linking between two chains [2,3]. The defect state induced by the C_3-C_3 dynamic bond appears close to the midgap. Following lattice relaxation, two unequally populated LP^1 sites that form upon excitation are converted into the LP^0 and LP^2 states; i.e., the charge transfer reaction $LP^1 + LP^1 \rightarrow LP^0 + LP^2$ is initiated since the system meets the requirement $|\Delta U_{EC}| > 2|\Delta U_{EB}|$. For the IVAP pair defect, the double excitation is found to induce bond rearrangements followed by the formation of the single C_3 defect with three equivalent bonds of 2.4–2.5 Å in length (the defect state appears closer to the conduction band). To reach the final configuration, the lattice relaxation requires overcoming the potential barrier $\Delta V_B \sim 0.8$ eV. It correlates well with the potential diagram presented in Fig. 3 for the $A^* \rightarrow C^*$ transition. Interestingly, an amorphous network can be resistant to the double-electron excitation if destabilization induced by a hole localized in the valence band tails is not enough to overcome the potential barrier ΔV_B. This is exactly the case for the two-chain VAP and single IVAP defects for which the B^* states with characteristic relaxation energy $\Delta U_{EB} \geq -0.1$ eV occur.

When the two missing electrons are returned into the system, the C^* state becomes unstable, and its stabilization requires breaking the dynamic or other bonds that depend on whether or not the dynamic bond is strongly stabilized at the excited state. The process of bond breaking and switching in the postexcitation regime occurs with the characteristic energy -0.9 ± 0.3 eV, which is similar to ΔU_{EC}. In this case, the final configuration is different from the original ground state A (Fig. 3) and is not necessarily the lowest in energy. The ideal system is converted into a system that contains a Se_7 ring, and a decrease in the total energy as compared with the initial configuration is found to be -0.49 eV. The IVAP pair [Fig. 2(c)] is converted into the double-chain VAP defect [Fig. 2(a)] accompanied by a lowering in energy by -0.28 eV. The achieved decrease in energy in both cases is larger than what the ringlike to helixlike transformations can provide (approximately -0.025 eV per atom [19]). This explains the predominant formation of the equilibrium centers such as the VAP defects upon excitation of the LP electrons.

Our simulations show that ringlike to helixlike transformations require a nucleation embryo, which is needed to recognize the symmetry of t-Se and, in such, to facilitate chain straightening. To confirm this, double-electron photoexcitation is simulated in a system with increased crystalline order (see Fig. 4). It is found to induce formation of the standard C_3-C_3 defect followed by chain straightening (see the excited state in Fig. 4), i.e., by ringlike to helixlike transformations. Because of the increased crystalline order of the initial system, the characteristic energies describing lattice relaxation during excitation $\Delta U_{EC} = -0.5 \pm 0.3$ eV are lower than that in the well-amorphized system.

In the postexcitation regime, the system with increased crystalline order completely converts to trigonal Se. A decrease in the total energy due to photocrystallization is found to be -0.08 eV, which agrees with the gain in energy provided by the ringlike to helixlike transformations involving up to five atoms (approximately ~ -0.025 eV

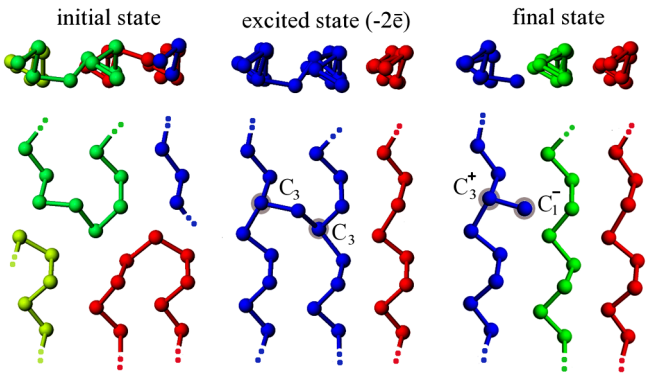

FIG. 4. The photoinduced crystallization of the increased crystalline order system. The final state is t-Se containing the IVAP defect.

per atom [19]). Therefore, we suggest that experimentally observed crystallization of the a-Se samples under sub-band-gap illumination [7,30] should be linked to the double-electron excitation process.

VI. THE STRUCTURAL TRANSFORMATIONS IN PD KINETICS

In order to verify that both single- and double-electron excitations are plausible processes involved in photoexcitation, the kinetics of PD in a temperature range between room temperature and 40 °C are studied experimentally (the upper temperature limit is dictated by an a-Se glass transition temperature [31,32]). The PD experiments are carried out on a 15-μm-thick a-Se layer (both pure a-Se and stabilized samples with 0.5% of As) using a standard two red laser beam setup (655 nm), where a powerful pump beam (150 mW/ cm^2) is used to produce photodarkening, while a very low intensity probe beam (0.29 mW/ cm^2) monitors the changes in the transmission of light T. The detailed descriptions of the experimental apparatus can be found in the previous work [6].

The kinetics of PD are studied by periodically exposing an a-Se sample to the pumping beam for 200 s separated by 200 s of rest. During those cycles, the probing beam transmission T is continuously monitored and relative changes in transmission T/T_0 are then calculated (T_0 is the initial transmission). The restoration of the transmission during the rest period at room temperature and selected elevated temperatures is shown in Fig. 5 and can be modeled by the double-exponential function yielding two characteristic time constants: τ_1 and τ_2. At room temperature, the characteristic relaxation times τ_1 and τ_2 derived from fitting of the resting cycles are 85 and 2.5 s, respectively, after averaging over several cycles.

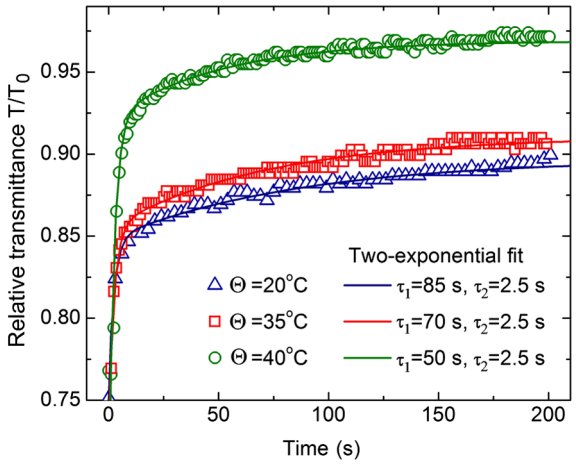

FIG. 5. Symbols: the experimental results on the PD relaxation in a-Se for three selected temperatures, namely, restoration of the probing beam transmission after switching off illumination (rest period). Solid lines: the fitted theoretical functions. Note: results are identical for pure and stabilized a-Se.

Remarkably, τ_1 decreases with an increase in temperature showing the Arrhenius dependence:

$$\tau_1 = \nu_0^{-1} \exp\left(\frac{E_B}{k_B \Theta}\right), \quad (1)$$

where k_B is the Boltzmann constant, Θ is the temperature, and ν_0 is the attempt-to-escape frequency. It yields the activation energy $E_B = 0.8 \pm 0.1$ eV ($\nu_0 = 2 \times 10^{11}$ s^{-1}). In contrast, τ_2 remains temperature independent for all applied temperatures.

The difference in the τ_1 and τ_2 behaviors indicates that the relaxation of PD involves two distinct processes: one that has the lattice relaxation in its origin and requires activation over a potential barrier with characteristic time τ_1, and another process which does not involve the lattice relaxation and occurs much faster with τ_2. The remarkable similarities between the magnitude of the activation energy $E_B = 0.8 \pm 0.1$ eV found in the PD experiment and $\Delta U_{EC} = -0.9 \pm 0.3$ eV required for the bond rearrangements makes us believe that this slow PD component describes the process of structural relaxation with the bond rearrangements. Therefore, the feasibility of the process of double-electron excitation accompanied by the formation of the LP^0 states is confirmed by the slow component of the PD relaxation. Taking into account two plausible scenarios for the LP^0 sites' formation ($LP^1 - \bar{e} \rightarrow LP^0$ or $LP^1 + LP^1 \rightarrow LP^0 + LP^2$), we suggest that the concentration of the LP^0 states should depend nonlinearly on the rate of excitation.

In contrast, the temperature independence of the fast component ($\tau_2 = 2.5$ s) is direct evidence of the relaxation process that does not involve bond rearrangements. It is consistent with very weak lattice relaxation $\Delta U_{EB} \geq -0.1$ eV involved in the stabilization of the LP^1 states generated by the single-electron excitation. The experimental detection of the unpaired electrons [2], which can be associated only with the LP^1 states, is further evidence of the single-electron excitation.

VII. CONCLUSIONS

The first-principles methods are applied to simulate the photoinduced structural transformations in an a-Se network and to compile a complete picture of the photoinduced changes. Our calculations suggest two distinct mechanisms of photoexcitation, i.e., single-electron and double-electron excitation, which are followed by different lattice relaxation processes. The excitation of a single electron from LP^2 leaves behind an unpaired electron and shifts the non-bonding LP^1 state towards the midgap, thus, inducing the photodarkening effect. This process manifests itself in the fast component of the relaxation of the photodarkening which is characterized by a short and temperature-independent characteristic time constant $\tau_2 = 2.5$ s. The fact that τ_2 is temperature independent suggests that no bond rearrangement is involved in lattice relaxation. Since

a hole localized at the LP^1 site does not trigger bond rearrangements, single-electron excitation cannot account for the photoinduced crystallization. However, it is responsible for the photoinduced volume expansion [10], as the LP^1 states appearing at the double-chain VAP defect increase a separation between the C_3^+ and C_1^- sites.

In order to trigger structural transformation in an *a*-Se network, excitation of two electrons from the vicinity of the same LP site is required. The characteristic energy of the lattice relaxation following the formation of the C_3-C_3 defect is found to be $\Delta U_{EC} = -0.9 \pm 0.3$ eV. This process is reflected in the slower component of the PD relaxation described by temperature-dependent time constant $\tau_1 = 85$ s yielding the activation energy $E_B = 0.8 \pm 0.1$ eV. The similarity between the characteristic energy ΔU_{EC}, which describes lattice transformation, and the activation energy E_B in the PD kinetics, suggests their identical origin. In addition, application of the double-electron excitation to a system of increased crystalline order is found to induce photocrystallization.

ACKNOWLEDGMENTS

The computational facilities have been acquired through membership in the Shared Hierarchical Academic Research Computing Network (SHARCNET [33]) and Compute/ Calcul Canada. The authors are also thankful to Dr. Safa Kasap for stimulating discussions and to Dr. O. Rubel for sharing his computational clusters. Financial support from the Ontario Research Fund-Research Excellence Program is highly acknowledged. The authors also acknowledge the Natural Sciences and Engineering Research Council of Canada (NSERC) and the Canadian Institutes of Health Research (CIHR) for financial support in the framework of a Collaborative Health Research Project.

[1] M. Kastner, D. Adler, and H. Fritzsche, Valence-alternation model for localized gap states in lone-pair semiconductors, Phys. Rev. Lett. **37**, 1504 (1976).

[2] A. V. Kolobov, M. Kondo, H. Oyanagi, A. Matsuda, and K. Tanaka, Negative correlation energy and valence alternation in amorphous selenium: An in situ optically induced ESR study, Phys. Rev. B **58**, 12004 (1998).

[3] A. Kolobov, H. Oyanagi, K. Tanaka, and K. Tanaka, Structural study of amorphous selenium by in situ EXAFS: Observation of photoinduced bond alternation, Phys. Rev. B **55**, 726 (1997).

[4] J. Rowlands and S. Kasap, Amorphous semiconductors usher in digital x-ray imaging, Phys. Today **50**, 24 (1997).

[5] S. R. Elliott, *Physics of Amorphous Materials* (Longman, Essex, 1990).

[6] A. Reznik, B. J. M. Lui, J. A. Rowlands, S. D. Baranovskii, O. Rubel, V. Lyubin, M. Klebanov, S. O. Kasap, Y. Ohkawa, T. Matsubara, K. Miyakawa, M. Kubota, K. Tanioka, and T. Kawai, Kinetics of the photostructural changes in a-Se films, J. Appl. Phys. **100**, 113506 (2006).

[7] R. E. Tallman, A. Reznik, B. A. Weinstein, S. D. Baranovskii, and J. A. Rowlands, Similarities in kinetics of photocrystallization and photodarkening in a-Se, Appl. Phys. Lett. **93**, 212103 (2008).

[8] A. Reznik, S. D. Baranovskii, M. Klebanov, V. Lyubin, O. Rubel, and J. A. Rowlands, Reversible vs irreversible photodarkening in a-Se: The kinetics study, J. Mater. Sci. Mater. Electron. **20**, S111 (2009).

[9] J. Hegedus, K. Kohary, D. G. Pettifor, K. Shimakawa, and S. Kugler, Photoinduced volume changes in amorphous selenium, Phys. Rev. Lett. **95**, 206803 (2005).

[10] K. Tanaka, Photoexpansion in As_2S_3 glass, Phys. Rev. B **57**, 5163 (1998).

[11] R. Lukács, S. D. Baranovskii, P. Thomas, and F. Gebhard, To the kinetics of photoinduced volume changes in chalcogenide glasses, J. Appl. Phys. **103**, 093541 (2008).

[12] K. Koughia and S. O. Kasap, Density of states of a-Se near the valence band, J. Non-Cryst. Solids **352**, 1539 (2006).

[13] K. Koughia, Z. Shakoor, S. O. Kasap, and J. M. Marshall, Density of localized electronic states in a-Se from electron time-of-flight photocurrent measurements, J. Appl. Phys. **97**, 033706 (2005).

[14] M. L. Benkhedir, M. Brinza, G. J. Adriaenssens, and C. Main, Structure of the band tails in amorphous selenium, J. Phys. Condens. Matter **20**, 215202 (2008).

[15] *Charge Transport in Disordered Solids*, edited by S. D. Baranovski (John Wiley & Sons, Ltd., Chichester, 2006), p. 156.

[16] K. Tanaka, Mechanisms of photodarkening in amorphous chalcogenides, J. Non-Cryst. Solids **59–60**, 925 (1983).

[17] P. Blaha, K. Schwarz, G. K. H. Madsen, D. Kvasnicka, and J. Luitz., *Wien2k: An Augmented Plane Wave+Local Orbitals Program for Calculating Crystal Properties: Karlheinz Schwarz* (Technische Universität, Wien, Austria, 2001).

[18] J. P. Perdew, K. Burke, and M. Ernzernof, Generalized gradient approximation made simple, Phys. Rev. Lett. **77**, 3865 (1996).

[19] K. Nakamura and A. Ikawa, Medium-range order in amorphous selenium: Molecular dynamics simulations, Phys. Rev. B **67**, 104203 (2003).

[20] X. Zhang and D. A. Drabold, Evidence for valence alternation, and a new structural model of amorphous selenium, J. Non-Cryst. Solids **241**, 195 (1998).

[21] R. Bellissent, Short range order in the disordered states of selenium-tellurium mixtures, Nucl. Instrum. Methods Phys. Res. **199**, 289 (1982).

[22] R. Lukács, M. Veres, K. Shimakawa, and S. Kugler, On photoinduced volume change in amorphous selenium: Quantum chemical calculation and Raman spectroscopy, J. Appl. Phys. **107**, 073517 (2010).

[23] T. Scopigno, W. Steurer, S. N. Yannopoulos, A. Chrissanthopoulos, M. Krisch, G. Ruocco, and T. Wagner, Vibrational dynamics and surface structure of amorphous selenium, Nat. Commun. **2**, 195 (2011).

[24] D. Hohl and R. O. Jones, First-principles molecular-dynamics simulation of liquid and amorphous selenium, Phys. Rev. B **43**, 3856 (1991).

[25] R. Steudel and E. -M. Strauss, Detection of Se_6, Se_7 and Se_8 in selenium solutions by high-pressure liquid chromatography, Z. Naturforsch **36B**, 1085 (1981).

[26] A. Roy, A. V. Kolobov, H. Oyanagi, and K. Tanaka, Photo-induced ring-to-chain conversion in as-evaporated films of amorphous selenium, Philos. Mag. B **78**, 87 (1998).

[27] S. N. Yannopoulos and K. S. Andrikopoulos, Raman scattering study on structural and dynamical features of noncrystalline selenium, J. Chem. Phys. **121**, 4747 (2004).

[28] C. K. Wong, G. Lucovsky, and J. Bernholg, Intrinsic localized defect states in a-Se associated with dihedral angle distortions, J. Non-Cryst. Solids **97–98**, 1171 (1987).

[29] G. Lucovsky, in *The Physics of Selenium and Tellerium*, edited by E. Gerlach and P. Grosse (Springer, New York, 1979), p. 178.

[30] A. Reznik, B. J. M. Lui, V. Lyubin, M. Klebanov, Y. Ohkawa, T. Matsubara, K. Miyakawa, M. Kubota, K. Tanioka, T. Kawai, and J. A. Rowlands, The effect of temperature on photoinduced metastability in avalanche a-Se layers, J. Non-Cryst. Solids **352**, 1595 (2006).

[31] S. O. Kasap and C. Juhasz, Kinematical transformations in amorphous selenium alloys used in xerography, J. Mater. Sci. **21**, 1329 (1986).

[32] J. P. Larmagnac, J. Grenet, and P. Michon, Glass transition temperature dependence on heating rate and on ageing for amorphous selenium films, J. Non-Cryst. Solids **45**, 157 (1981).

[33] http://www.sharcnet.ca.